The quasi-one-dimensional antiferromagnet $CsMnCl_3.2H_2O$. I. A random-phase approximation model

1989 J. Phys.: Condens. Matter 1 179

(http://iopscience.iop.org/0953-8984/1/1/016)

J. Phys.: Condens. Matter 1 (1989) 179–202. Printed in the UK

The quasi-one-dimensional antiferromagnet $CsMnCl_3 \cdot 2H_2O$: I. A random-phase approximation model

G J Bowden and J P D Martin
School of Physics, University of New South Wales, Kensington, NSW 2033, Australia

Received 13 April 1988

Abstract. A self-consistent random-phase approximation model has been used to simulate the magnetic properties of quasi-one-dimensional and three-dimensional antiferromagnets at low temperatures, and in various applied fields. To avoid problems associated with crystal-field terms, we have replaced the quadratic $D[S_z^2 - \frac{1}{2}S(S+1)]$ term, which is responsible for easy-axis alignment, with anisotropic magnetic exchange. The resultant calculations have been used to discuss sublattice magnetisation, specific heats and nuclear–magnon coupling, in various applied fields, particularly near the antiferromagnetic–paramagnetic phase transition. Our principal conclusion is that magnetic moments in quasi-one-dimensional antiferromagnetic moments are likely to be characterised by a large zero-point motion. This feature has important implications for nuclear orientation experiments in the milli-kelvin regime.

1. Introduction

In recent years, the magnon heat switch in insulating antiferromagnetic compounds has been used to reach previously unattainable nuclear spin temperatures in the milli-kelvin regime (Allsop *et al* 1984). Simply by applying a magnetic field along the easy axis of an antiferromagnetic compound, it is possible to cool the nuclei, by bringing them into contact with the magnon and phonon heat reservoirs. In general, nuclear spin temperatures are higher than those of the magnon and phonon heat baths, because of the long nuclear spin relaxation times T_1 encountered in the milli-kelvin regime. Fortunately this thermal bottleneck can be bypassed by applying the so-called spin-flop field B_{sf} along the easy magnetic axis of the antiferromagnetic compound. This effectively reduces the energy gap in the magnon dispersion curve to zero, thereby allowing the nuclei and magnons to exchange energy freely via the off-diagonal elements in the nuclear hyperfine interaction $AI \cdot S$. Concomitantly, it is possible to isolate the nuclei, once they have been cooled, by simply removing the magnetic field. These two features allow both nuclear orientation (NO) and nuclear magnetic resonance on oriented nuclei (NMRON) to be carried out rapidly, and with high sensitivity (e.g. Allsop *et al* 1984). Recently, for example, the magnon heat switch has been employed in pulsed ^{54}Mn NMRON experiments by Turrell *et al* (1987), and by Bowden *et al* (1987) in their study of ^{54}Mn NMR enhancement factors in $MnCl_2 \cdot 4H_2O$ as a function of applied field.

In all of the previously mentioned investigations, however, only two three-

0953-8984/89/010179 + 24 $02.50

dimensional (3D) antiferromagnetic salts $MnCl_2 \cdot 4H_2O$ and $MnBr_2 \cdot 4H_2O$ have been examined in any detail. In essence, these two antiferromagnetic compounds are characterised by exchange interactions which are roughly of the same order of magnitude in all three principal directions. Turrell (1985) has reported some preliminary data on the two-dimensional antiferromagnetic salt $Mn(COOCH)_2 \cdot 4H_2O$, where the exchange parameter J_a along the a axis is some one-thousandth of the strength of the exchange parameters along the b and c axes. However, to our knowledge, no NO or NMRON results have been reported for one-dimensional (1D) antiferromagnetic salts. This class of one-dimensional antiferromagnetic salts is expected to show unusual behaviour, as noted for example in the review article by de Groot and de Jongh (1986). Moreover, it is also of interest to enquire whether or not the 'magnon heat switch' can also be used in quasi-1D antiferromagnetic insulators, alternately both to cool and to isolate the nuclei.

With these ideas in mind, therefore, we have carried out a special study on the one-dimensional antiferromagnet $CsMnCl_3 \cdot 2H_2O$. This compound orders at 4.88 K (Butterworth *et al* 1973) and possesses a spin-flop field B_{sf} of 1.68(2) T (this work). To all intents and purposes therefore, $CsMnCl_3 \cdot 2H_2O$ is very similar to the 3D antiferromagnet $MnCl_2 \cdot 4H_2O$, where $T_N = 1.62$ K and $B_{sf} = 0.72$ T (Rives and Benedict 1975). However both the specific heat studies in Kopinga *et al* (1975) and the neutron scattering data reported in Skalyo *et al* (1970a, b) reveal that the strength of the exchange parameter J_a, along the a axis of the orthorhombic structure, is some 300 times stronger than that along the b and c axes. Thus this compound should be representative of one-dimensional antiferromagnetic insulators.

In this, the first of two papers (hereafter referred to as I), we present some theoretical calculations for one-dimensional antiferromagnetic insulators. We have chosen to present our theoretical calculations first because it is believed that the conclusions reached during this stage of our work have an important bearing on the interpretation of the experimental data presented in the following paper (Bowden *et al* 1989, which we shall refer to as II). In particular, it will be argued that one-dimensional antiferromagnetic insulators are likely to be characterised by a very large zero-point motion (~30%). Thus attempts to interpret the NO data from quasi-1D antiferromagnetic insulators, using spin-wave theory (see for example Gladkov 1986a, b), are unlikely to succeed.

The structure of this paper is as follows. In § 2, the various mathematical approaches that can be used to investigate the nuclear–magnon interaction in the strongly coupled regime are reviewed. In §§ 3 and 4, full details are given of the random-phase approximation (RPA) model, used to compute ensemble averages such as the magnetisation, etc., in various applied fields. In particular, a modification to the usual low-temperature spin-wave approximation is presented which can be used to calculate both the entropy and specific heat right up to the Néel temperature T_N.

2. Mathematical preliminaries

As mentioned earlier, the nuclei and magnons in an easy-axis antiferromagnetic salt become strongly coupled when the applied magnetic field is raised to the spin-flop value B_{sf}. Thus the use of spin-wave theory (e.g. Gladkov 1986a, b), and or perturbative methods, must fail near B_{sf}. Further, it will be shown in this paper that one-dimensional antiferromagnets, in zero applied field and at zero temperature, are characterised by

considerable zero-point motion of the magnetic ions. We therefore seek a model that can accommodate, *ab initio*, large deviations from magnetic saturation in both the nuclear and electronic antiferromagnetic sublattices.

Of the models available, the random-phase approximation (RPA) appears to be most suitable. This model can be used, at least in principle, to compute self-consistent observables over the whole range from $0 \leqslant B_{app} \leqslant B_{sf}$. Further, in the limit $T \rightarrow 0$ K, it is well known that the results of the RPA model reduce to those of spin-wave theory, at least in 3D antiferromagnets (Keffer 1966). However there are problems.

In the first place, it is not possible to model accurately even a simple two-electronic-sublattice antiferromagnet, subject to both antiferromagnetic exchange and crystal-field interactions. In general, easy-axis insulating antiferromagnets such as $MnCl_2 \cdot 4H_2O$ are well described by a simple Hamiltonian

$$\mathcal{H} = -\tfrac{1}{2} \sum_{\{i,j\}} J_{ij} \boldsymbol{J}(i) \cdot \boldsymbol{J}(j) + \sum_i D[(J_z(i))^2 - J(J+1)/3] \tag{1}$$

where J_{ij} is an isotropic exchange parameter and D is a simple quadratic crystal-field parameter which constrains the spins to point along the easy magnetic axis. However, in practice crystal-field interactions are not easily incorporated into the RPA. This problem has been discussed by Egami and Brooks (1975), Haley (1978) and more recently by Bowden *et al* (1986). Unfortunately, the use of the RPA, to reduce the number of coupled Green functions to a manageable level, leads to inconsistencies in the calculation of ensemble averages. However, unlike single-ion crystal-field anisotropy, anisotropic magnetic exchange, which mimics the easy alignment of the magnetic ions, can be easily incorporated into the RPA approximation with no inconsistencies. In this paper therefore, we shall replace equation (1) with

$$\mathcal{H} = -\tfrac{1}{2} \sum_{\{i,j\}} J_{ij} \boldsymbol{J}(i) \cdot \boldsymbol{J}(j) - \tfrac{1}{2} \sum_{[i,j\}} K_{ij} J_z(i) J_z(j). \tag{2}$$

This approximation means of course that exact agreement with experiment and the predictions of the RPA model cannot and should not be expected. Nevertheless, we believe that the results obtained using equation (2) represent a good first approximation to this difficult problem.

On a more positive note, it is possible, within the RPA, to compute self-consistent Fano statistical tensors (ensemble averages) using the recursion relationships given by Bowden *et al* (1986). These relationships, originally derived for an ordered nuclear ferromagnet, still hold regardless of the number of collinear magnetically coupled sublattices. Consequently, it is a relatively easy matter to extend the calculation for a simple two-sublattice electronic antiferromagnet to one that includes two nuclear sublattices. The latter calculations are of course of great interest in the interpretation of nuclear orientation (NO) results, where the γ-ray anisotropy pattern is dictated primarily by the nuclear Fano statistical tensor ρ_0^2.

Finally, before leaving this section it should be noted that the operators used in the remainder of this paper are not the Cartesian operators $\boldsymbol{J}_x, \boldsymbol{J}_y, \boldsymbol{J}_z$, etc, used in equations (1) and (2), but rather unit irreducible tensor operators $\hat{T}_q^n$. In decoupling Green function equations, irreducible tensor operators are much more convenient to use in practice because of their contraction properties. All the terminology used in this paper therefore closely follows that of Bowden *et al* (1986).

3. Green function theory applied to a simple two-sublattice antiferromagnet

In terms of unit tensor operators for both the electronic and nuclear spins, the Hamiltonian in question can be written in the form

$$\begin{aligned}\mathcal{H} = &-\tfrac{1}{2}\sum_{\{i,j\}} \alpha^2(S)J_{ij}[\hat{T}^1_0(i)\hat{T}^1_0(j) - \hat{T}^1_1(i)\hat{T}^1_{-1}(j) - \hat{T}^1_{-1}(i)\hat{T}^1_1(j)] \\ &- \tfrac{1}{2}\sum_{\{i,j\}} \alpha^2(S)K_{ij}\hat{T}^1_0(i)\hat{T}^1_0(j) - \alpha(S)g_{\mu B}B_{\text{app}}\left(\sum_i \hat{T}^1_0(i) + \sum_j \hat{T}^1_0(j)\right) \\ &- \alpha(I)g_N\mu_N B_{\text{app}}\left(\sum_i \hat{L}^1_0(i) + \sum_j \hat{L}^1_0(j)\right) \\ &+ \alpha(S)\alpha(I)A\left(\sum_i [\hat{T}^1_0(i)\hat{L}^1_0(i) - \hat{T}^1_1(i)\hat{L}^1_{-1}(i) - \hat{T}^1_{-1}(i)\hat{L}^1_1(i)]\right. \\ &\left.+ \sum_j [\hat{T}^1_0(j)\hat{L}^1_0(j) - \hat{T}^1_1(j)\hat{L}^1_{-1}(j) - \hat{T}^1_{-1}(j)\hat{L}^1_1(j)]\right) \qquad (3)\end{aligned}$$

where (i) $\hat{T}^n_q$ ($\hat{L}^{n'}_{q'}$) refers to the electronic (nuclear) unit tensor operators, respectively, (ii) J_{ij} describes the isotropic exchange interaction (negative for antiferromagnets), (iii) K_{ij} is the anisotropic exchange which mimics easy-axis alignment, (iv) A is the hyperfine interaction parameter (negative for Mn nuclei) and (v)

$$\alpha(S) = 1/[12(2S-1)!/(2S+2)!]^{1/2} \qquad (4)$$

where S is the spin of the electronic moment. In Mn^{2+} antiferromagnets, the hyperfine interaction $A\boldsymbol{I}\cdot\boldsymbol{S}$ is the dominant term in the nuclear Hamiltonian, and so we shall ignore any nuclear quadrupole interactions, nuclear spin–spin coupling, etc.

As noted earlier, once the eigenvalues and expectation values $\langle\hat{T}^n_q\rangle$ and $\langle\hat{L}^n_q\rangle$ have been calculated within the RPA, it is possible to derive thermodynamic quantities such as sublattice magnetisation, etc, even in the strongly coupled regime. For example, for NO experiments the required statistical tensors are given by $\rho^n_q = (-1)^n\langle\hat{L}^n_q\rangle$, where the $(-1)^n$ has been inserted to bring about agreement between our work and that of Steffen and Alder (1975).

4. Two-sublattice electronic antiferromagnet: $A = 0$

Before embarking on a discussion of the general case, it is instructive first to consider the case of a simple antiferromagnet with no hyperfine interactions. Using standard Green function theory (Zubarev 1960) (see also equations (17) and (18) from Bowden *et al* (1986)), and taking the site 1 to be on sublattice (1), it can be shown that the appropriate Green function equation of motion for sublattice (1) is given by

$$\begin{aligned}E\langle\langle\hat{T}^1_1(l);\hat{T}^n_{q-1}(m)\rangle\rangle = &\, c_1\langle\hat{T}^n_q(m)\rangle\delta_{l,m}/(2\pi) + g\mu_B B_{\text{app}}\langle\langle\hat{T}^1_1(l);\hat{T}^n_{q-1}(m)\rangle\rangle \\ &+ \alpha(S)\sum_{j\neq l}\{(J_{ij}+K_{ij})\langle\langle[\hat{T}^1_1(l)\hat{T}^1_0(j);\hat{T}^n_{q-1}(m)\rangle\rangle \\ &- J_{ij}\langle\langle\hat{T}^1_0(l)\hat{T}^1_1(j);\hat{T}^n_{q-1}(m)\rangle\rangle\} \qquad (5)\end{aligned}$$

where (i) $\alpha(S)$ is given by equation (4) and (ii)

$$c_1 = -[(n+q)(n-q+1)/2]^{1/2}/\alpha(S). \tag{6}$$

In practice, only equations with $q = 0$ are non-zero in our RPA model. However, for generality, we shall continue to write down the Green function equations for general q.

If only nearest-neighbour (NN) interactions between alternate sublattices (1) and (2) are allowed, the equation of motion in the RPA approximation reduces to

$$\begin{aligned} E\langle\langle \hat{T}_1^1(l); \hat{T}_{q-1}^n(m)\rangle\rangle &= c_1\langle \hat{T}_q^n(m)\rangle\delta_{l,m}/(2\pi) + g\mu_B B_{app}\langle\langle \hat{T}_1^1(l); \hat{T}_{q-1}^n(m)\rangle\rangle \\ &+ \alpha(S)\sum_{j\neq l}(J_{ij}+K_{ij})\langle \hat{T}_0^1(j)\rangle\langle\langle \hat{T}_1^1(l); \hat{T}_{q-1}^n(m)\rangle\rangle \\ &- \alpha(S)\sum_{j\neq l} J_{ij}\langle \hat{T}_0^1(l)\rangle\langle\langle \hat{T}_1^1(j); \hat{T}_{q-1}^n(m)\rangle\rangle. \end{aligned} \tag{7}$$

Note that in this equation $\langle \hat{T}_0^1(l)\rangle$ and $\langle \hat{T}_0^1(j)\rangle$ are distinct, as l and j belong to the two different sublattices. Consequently, a second equation of motion must be obtained for $\langle\langle \hat{T}_1^1(p); \hat{T}_{q-1}^n(m)\rangle\rangle$ where p is located on sublattice (2). We find

$$\begin{aligned} E\langle\langle \hat{T}_1^1(p); \hat{T}_{q-1}^n(m)\rangle\rangle &= c_1\langle \hat{T}_q^n(m)\rangle\delta_{p,m}/(2\pi) + g\mu_B B_{app}\langle\langle \hat{T}_1^1(p); \hat{T}_{q-1}^n(m)\rangle\rangle \\ &+ \alpha(S)\sum_{i\neq p}(J_{pi}+K_{pi})\langle \hat{T}_0^1(i)\rangle\langle\langle \hat{T}_1^1(p); \hat{T}_{q-1}^n)\rangle\rangle \\ &- \alpha(S)\sum_{i\neq p} J_{pi}\langle \hat{T}_0^1(p)\rangle\langle\langle \hat{T}_1^1(i); \hat{T}_{q-1}^n(m)\rangle\rangle. \end{aligned} \tag{8}$$

Thus the problem has been reduced to solving two coupled Green function equations. Note that the two delta functions $\delta_{l,m}$ and $\delta_{p,m}$ cannot simultaneously be equal to unity because l and p are on separate sublattices.

Spatial Fourier-transform methods can be used to solve equations (7) and (8) for $\langle \hat{T}_q^n\rangle_{1,2}$ (e.g. Zubarev 1960). Following Bowden *et al* (1986), we write

$$E\mathbf{G} = \mathbf{MG} + \mathbf{T} \tag{9}$$

where (i) $\mathbf{G}$ is the Green function matrix

$$\mathbf{G} = \begin{pmatrix} G_{11}^{ee}(E,k) & G_{12}^{ee}(E,k) \\ G_{21}^{ee}(E,k) & G_{22}^{ee}(E,k) \end{pmatrix} \tag{10}$$

(ii) the matrix $\mathbf{M}$ is given by

$$\mathbf{M} = \begin{pmatrix} g\mu_B B_{app} + \alpha(S)\langle \hat{T}_0^1\rangle_2[J(0)+K(0)] & -\alpha(S)\langle \hat{T}_0^1\rangle_2 J_{21}(-k) \\ -\alpha(S)\langle \hat{T}_0^1\rangle_1 J_{12}(k) & g\mu_B B_{app} + \alpha(S)\langle \hat{T}_0^1\rangle_1[J(0)+K(0)] \end{pmatrix} \tag{11}$$

and (iii)

$$\mathbf{T} = \begin{pmatrix} c_1\langle \hat{T}_q^n\rangle_1/(2\pi) & 0 \\ 0 & c_1\langle \hat{T}_q^n\rangle_2/(2\pi) \end{pmatrix}. \tag{12}$$

The four Green functions $G_{11}^{ee}(E,k)$, $G_{21}^{ee}(E,k)$, $G_{21}^{ee}(E,k)$ and $G_{22}^{ee}(E,k)$ and the Fourier transforms $J_{12}(k)$ and $J_{21}(-k)$ are defined in table 1. The $\langle \hat{T}_0^1\rangle_{1,2}$ are the self-consistent ensemble averages of $\hat{T}_0^1$ for the two sublattices (1) and (2), as noted earlier.

Table 1. Definition of electronic, nuclear and mixed electronic and nuclear Green functions[a].

$$J_{12}(k) = \sum_{j \neq l} J_{ij} \exp[-\mathrm{i}\boldsymbol{k} \cdot (\boldsymbol{R}_l - \boldsymbol{R}_j)]$$

$$J_{21}(-k) = \sum_{i \neq p} J_{pi} \exp[-\mathrm{i}\boldsymbol{k} \cdot (\boldsymbol{R}_p - \boldsymbol{R}_i)]$$

$$G_{11}^{\mathrm{ee}}(E,k) = \sum_m \langle\langle \hat{T}_1^1(l); \hat{T}_{q-1}^n(m) \rangle\rangle \exp[-\mathrm{i}\boldsymbol{k} \cdot (\boldsymbol{R}_l - \boldsymbol{R}_m)]$$

$$G_{12}^{\mathrm{ee}}(E,k) = \sum_m \langle\langle \hat{T}_1^1(p); \hat{T}_{q-1}^n(m) \rangle\rangle \exp[-\mathrm{i}\boldsymbol{k} \cdot (\boldsymbol{R}_p - \boldsymbol{R}_m)]$$

$$G_{21}^{\mathrm{ee}}(E,k) = \sum_n \langle\langle \hat{T}_1^1(l); \hat{T}_{q-1}^n(n) \rangle\rangle \exp[-\mathrm{i}\boldsymbol{k} \cdot (\boldsymbol{R}_l - \boldsymbol{R}_n)]$$

$$G_{22}^{\mathrm{ee}}(E,k) = \sum_n \langle\langle \hat{T}_1^1(p); \hat{T}_{q-1}^n(n) \rangle\rangle \exp[-\mathrm{i}\boldsymbol{k} \cdot (\boldsymbol{R}_p - \boldsymbol{R}_n)]$$

$$G_{11}^{\mathrm{ne}}(E,k) = \sum_m \langle\langle \hat{L}_1^1(l); \hat{T}_{q-1}^n(m) \rangle\rangle \exp[-\mathrm{i}\boldsymbol{k} \cdot (\boldsymbol{R}_l - \boldsymbol{R}_m)]$$

$$G_{12}^{\mathrm{ne}}(E,k) = \sum_m \langle\langle \hat{L}_1^1(p); \hat{T}_{q-1}^n(m) \rangle\rangle \exp[-\mathrm{i}\boldsymbol{k} \cdot (\boldsymbol{R}_p - \boldsymbol{R}_m)]$$

$$G_{21}^{\mathrm{ne}}(E,k) = \sum_n \langle\langle \hat{L}_1^1(l); \hat{T}_{q-1}^n(n) \rangle\rangle \exp[-\mathrm{i}\boldsymbol{k} \cdot (\boldsymbol{R}_l - \boldsymbol{R}_n)]$$

$$G_{22}^{\mathrm{ne}}(E,k) = \sum_n \langle\langle \hat{L}_1^1(p); \hat{T}_{q-1}^n(n) \rangle\rangle \exp[-\mathrm{i}\boldsymbol{k} \cdot (\boldsymbol{R}_p - \boldsymbol{R}_n)]$$

$$G_{11}^{\mathrm{en}}(E,k) = \sum_m \langle\langle \hat{T}_1^1(l); \hat{L}_{q-1}^n(m) \rangle\rangle \exp[-\mathrm{i}\boldsymbol{k} \cdot (\boldsymbol{R}_l - \boldsymbol{R}_m)]$$

$$G_{12}^{\mathrm{en}}(E,k) = \sum_m \langle\langle \hat{T}_1^1(p); \hat{L}_{q-1}^n(m) \rangle\rangle \exp[-\mathrm{i}\boldsymbol{k} \cdot (\boldsymbol{R}_p - \boldsymbol{R}_m)]$$

$$G_{21}^{\mathrm{en}}(E,k) = \sum_n \langle\langle \hat{T}_1^1(l); \hat{L}_{q-1}^n(n) \rangle\rangle \exp[-\mathrm{i}\boldsymbol{k} \cdot (\boldsymbol{R}_l - \boldsymbol{R}_n)]$$

$$G_{22}^{\mathrm{en}}(E,k) = \sum_n \langle\langle \hat{T}_1^1(p); \hat{L}_{q-1}^n(n) \rangle\rangle \exp[-\mathrm{i}\boldsymbol{k} \cdot (\boldsymbol{R}_p - \boldsymbol{R}_n)]$$

$$G_{11}^{\mathrm{nn}}(E,k) = \sum_m \langle\langle \hat{L}_1^1(l); \hat{L}_{q-1}^n(m) \rangle\rangle \exp[-\mathrm{i}\boldsymbol{k} \cdot (\boldsymbol{R}_l - \boldsymbol{R}_m)]$$

$$G_{12}^{\mathrm{nn}}(E,k) = \sum_m \langle\langle \hat{L}_1^1(p); \hat{L}_{q-1}^n(m) \rangle\rangle \exp[-\mathrm{i}\boldsymbol{k} \cdot (\boldsymbol{R}_p - \boldsymbol{R}_m)]$$

$$G_{21}^{\mathrm{nn}}(E,k) = \sum_n \langle\langle \hat{L}_1^1(l); \hat{L}_{q-1}^n(n) \rangle\rangle \exp[-\mathrm{i}\boldsymbol{k} \cdot (\boldsymbol{R}_l - \boldsymbol{R}_m)]$$

$$G_{22}^{\mathrm{nn}}(E,k) = \sum_n \langle\langle \hat{L}_1^1(p); \hat{L}_{q-1}^n(n) \rangle\rangle \exp[-\mathrm{i}\boldsymbol{k} \cdot (\boldsymbol{R}_p - \boldsymbol{R}_n)]$$

[a] l and m refer to sublattice (1); p and n refer to sublattice (2).

On solving equation (9) we find

$$G_{11}^{\mathrm{ee}}(E,k) = c_1 \frac{\langle \hat{T}_q^n \rangle_1}{2\pi} \frac{E - \{g\mu_{\mathrm{B}} B_{\mathrm{app}} + \alpha(S)\langle \hat{T}_0^1 \rangle_1 [J(0) + K(0)]\}}{(E - E_{1k})(E - E_{2k})} \tag{13}$$

$$G_{22}^{\mathrm{ee}}(E,k) = c_1 \frac{\langle \hat{T}_q^n \rangle_2}{2\pi} \frac{E - \{g\mu_{\mathrm{B}} B_{\mathrm{app}} + \alpha(S)\langle \hat{T}_0^1 \rangle_2 [J(0) + K(0)]\}}{(E - E_{1k})(E - E_{2k})} \tag{14}$$

where the poles of the Green functions are given by det $\mathbf{M} = 0$. Explicitly

$$E_{1k,2k} = g\mu_B B_{app} + \alpha(S)\{\tfrac{1}{2}(\langle\hat{T}_0^1\rangle_1 + \langle\hat{T}_0^1\rangle_2)[J(0) + K(0)] \pm \tfrac{1}{2}[(\langle\hat{T}_0^1\rangle_1 - \langle\hat{T}_0^1|_2)^2[J(0) + K(0)]^2 + 4\langle\hat{T}_0^1\rangle_1\langle\hat{T}_0^1\rangle_2 J_{12}(k)J_{21}(-k)]^{1/2}\}. \quad (15)$$

Note that if we make the assumption that $\alpha(S)\langle\hat{T}_0^1\rangle_1 = -\alpha(S)\langle\hat{T}_0^1\rangle_2 = S$ at absolute zero, then equation (15) reduces to

$$E_{1k,2k} = g\mu_B B_{app} \pm S\{[J(0) + K(0)]^2 - J(k)^2\}^{1/2} \quad (16)$$

which is the well known spin-wave result for antiferromagnetic magnons in cubic symmetry. In practice, of course, both the ensemble averages $\langle\hat{T}_0^1\rangle_1$ and $\langle\hat{T}_0^1\rangle_2$ in an antiferromagnet are less than the saturated value $S/\alpha(S)$, as a result of zero-point motion (Keffer 1966).

Given equations (13)–(15), self-consistent values of $\langle\hat{T}_q^n\rangle_{1,2}$ can be obtained in an iterative manner. In practice, this is achieved by performing the inverse Fourier transforms

$$\langle\langle\hat{T}_1^1(l); \hat{T}_{q-1}^n(m)\rangle\rangle = 2N^{-1}\sum_k G_{11}(E, k)\exp[+i\boldsymbol{k}\cdot(\boldsymbol{R}_l - \boldsymbol{R}_m)] \quad (17)$$

$$\langle\langle\hat{T}_1^1(p); \hat{T}_{q-1}^n(n)\rangle\rangle = 2N^{-1}\sum_k G_{22}(E, k)\exp[+i\boldsymbol{k}\cdot(\boldsymbol{R}_p - \boldsymbol{R}_n)] \quad (18)$$

and subsequently employing the spectral theorem, as detailed by Zubarev (1960). The equilibrium correlation functions of the two sublattices are then obtained via the equations

$$\langle\hat{T}_{q-1}^n\hat{T}_1^1\rangle_1 = c_1\langle\hat{T}_q^n\rangle_1\varphi_1 \quad (19)$$

$$\langle\hat{T}_{q-1}^n\hat{T}_1^1\rangle_2 = c_1\langle\hat{T}_q^n\rangle_2\varphi_2 \quad (20)$$

where (i)

$$\varphi_{1,2} = \frac{2}{N}\sum_k\left(\frac{r_{1,2}(k)}{\exp(\beta E_{1k}) - 1} + \frac{1 - r_{1,2}(k)}{\exp(\beta E_{2k}) - 1}\right) \quad (21)$$

and (ii)

$$r_{1,2}(k) = \frac{E_{1k} - \{g\mu_B B_{app} + \alpha(S)\langle\hat{T}_0^1\rangle_{1,2}[J(0) + K(0)]\}}{E_{1k} - E_{2k}} \quad (22)$$

respectively. The $E_{1k,2k}$ of course are given by the self-consistent solution of equation (15).

In practice, it can be shown that the functional form of equations (19) and (20) is exactly the same as that found for simple ferromagnets (see equation (24) of Bowden *et al* (1986)). Thus the recursion relationships and expressions for the $\langle\hat{T}_q^n\rangle$ given by these authors also apply here, the only quantitative difference being that of the new weighting factors φ_1 and φ_2, which reflect the presence of two coupled magnon branches.

Using equations (5)–(22), calculations of the sublattice magnetisations, entropy and specific heat for the model antiferromagnetic system have been carried out. Of particular interest is the behaviour of these parameters near the field-induced phase transition. The calculations presented below are for the specific case of $S = \frac{5}{2}$, which corresponds to the spin of the Mn^{2+} ion.

4.1. Sublattice magnetisation: A = 0

From table 2 of Bowden *et al* (1986), the sublattice magnetisations are given by

$$\langle \hat{T}_0^1 \rangle_1 = \frac{5 + 28\varphi_1 + 63\varphi_1^2 + 70\varphi_1^3 + 35\varphi_1^4}{\sqrt{70}[(1+\varphi_1)^6 - \varphi_1^6]} \tag{23}$$

and

$$\langle \hat{T}_0^1 \rangle_2 = \frac{5 + 28\varphi_2 + 63\varphi_2^2 + 70\varphi_2^3 + 35\varphi_2^4}{\sqrt{70}[(1+\varphi_2)^6 - \varphi_2^6]} \tag{24}$$

for $S = \frac{5}{2}$. Both these values of $\langle \hat{T}_0^1 \rangle_1$ and $\langle \hat{T}_0^1 \rangle_2$ exhibit zero-point motion of the ground state at $T = 0$ K, a characteristic property of antiferromagnets.

Before calculating the self-consistent values of $\langle \hat{T}_0^1 \rangle_{1,2}$, it is necessary to specify the spin structure of the antiferromagnetic compound, since the magnon dispersion term $J_{12}(k)$ depends explicitly on the spatial arrangement of nearest neighbours. For the purposes of this paper it will be assumed that the model antiferromagnet consists of two interpenetrating face-centred-cubic lattices. This results in a simple cubic arrangement of the nearest neighbours, of distance a (Å), about any particular ion. Consequently, following Kubo (1952), we find

$$J_{3D}(k) = J_{3D}(-k) = J_{3D}(0)\,[\cos(k_x a) + \cos(k_y a) + \cos(k_z a)]/3 \tag{25}$$

for isotropic 3D exchange, while

$$J_{Q1D}(k) = J_{Q1D}(-k) = J_{Q1D}(0)\{\eta[\cos(k_x a) + \cos(k_y a)] + \cos(k_z a)\}/(1 + 2\eta) \tag{26}$$

for quasi-1D exchange, where $\eta \ll 1$.

Fortunately, the required computation can be reduced by exploiting the symmetry of the Brillouin zone. For the isotropic 3D exchange an irreducible one-forty-eighth of the zone is required. For the quasi-1D exchange, however, one-sixteenth of the zone is required, as a result of the lower symmetry. In addition, it should be noted that in practice the real mesh of N k-space values is replaced by a coarser grid of n points

$$N^{-1} \sum_k f(k) \rightarrow n^{-1} \sum_i f(\xi_i) \tag{27}$$

where the ξ_i are the points in the new grid system. Thus the RPA calculations for φ_1 and φ_2 were not carried out using equation (21), but rather

$$\varphi_{1,2} = \frac{2}{n} \sum_q W(q) \left(\frac{r_{1,2}(q)}{\exp(\beta E_{1q}) - 1} + \frac{1 - r_{1,2}(q)}{\exp(\beta E_{2q}) - 1} \right) \tag{28}$$

where (i) n was usually set at 7110 for both the 3D and quasi-1D antiferromagnets and (ii) the weighting factors $W(q)$ account for any degeneracies at each point q in the respective irreducible zones. Thus the total number of points sampled in k-space was 8×7110. Note that since the first Brillouin zone is a truncated octahedron, the summations along any direction must cease when the boundaries

$$k_x a, k_y a, k_z a = \pi \qquad \text{and} \qquad |k_x a| + |k_y a| + |k_z a| = 1.5\pi \tag{29}$$

are exceeded.

Self-consistent calculations of the sublattice magnetisations, in zero applied field, as a function of temperature may be seen in figure 1 for a 3D and quasi-1D antiferromagnet.

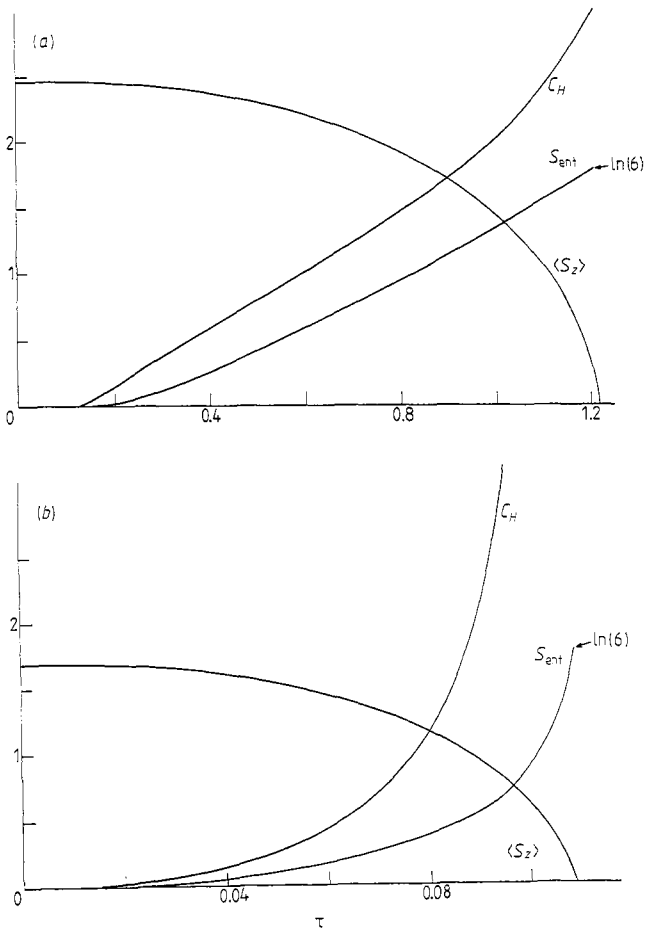

Figure 1. The calculated magnetisation, entropy and specific heat results for a 3D antiferromagnet (a), with $S = 5/2$ and $(J(0) + K(0))/J(0) = 1.233$, and a quasi-1D antiferromagnet (b), with $S = 5/2$ and $(J(0) + K(0))/J(0) = 1.00215$, in the absence of nuclei.

The choice of the $[J(0) + K(0)]/J(0)$ ratios used in these calculations was dictated primarily by the measured values of the exchange field B_E^{eff} and the anisotropy field B_A in $MnCl_2 \cdot 4H_2O$ and $CsMnCl_3 \cdot 2H_2O$ respectively (Bowden *et al* 1987, II). Since (i) these parameters were obtained using a mean-field Hamiltonian and (ii) the simple cubic lattice does not truly represent the two compounds in question, only semi-quantitative agreement with experiment should be expected, as noted earlier.

From an examination of figure 1, it will be observed that the temperature scale has been expressed in dimensionless units τ, where

$$\tau = k_B T / g\mu_B B_E^{eff} \tag{30}$$

and $g\mu_B B_E^{eff} = SJ(0)$. Thus if either T or B_E^{eff} is known then the other quantity can be calculated. For example using $B_E^{eff} = 1.099$ T for $MnCl_2 \cdot 4H_2O$ (see Bowden *et al* 1987), and $\tau_N = 1.216$ from figure 1(a), equation (30) reveals that $T = 1.795$ K. The difference between this estimate and the observed T_N of 1.62 K presumably results from a combination of the use of molecular-field parameters, an incorrect lattice structure, magnetic

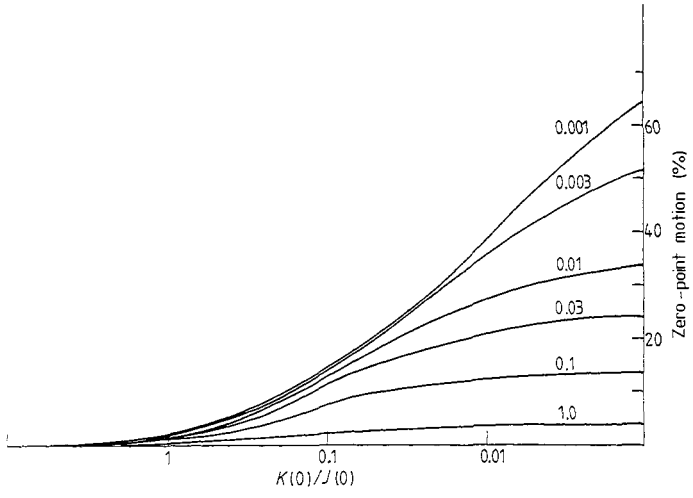

Figure 2. The calculated zero-point motion, $[1 - \langle S_z \rangle / S]$, of an antiferromagnet as a function of the magnetic exchange ratio $\eta = (J_a/J_b)$ (the numbers against the curves are values of $1/\eta$), and the anisotropic magnetic exchange parameter $K(0)/J(0)$.

anisotropy in place of crystal-field alignment and the RPA approximation used in the many-body model. Another approach to the problem would be to fit both τ_N and the spin-flop field transition to the experimental data. In this way $J(0)$ and $K(0)$ could be obtained directly. However, since our model only exhibits an antiferromagnetic–paramagnetic (AF–P) transition, no progress can be made in this direction.

From an examination of the two-sublattice magnetisations shown in figure 1, the most obvious difference to emerge between quasi-1D and 3D antiferromagnets is the appearance of large zero-point motion in the quasi-1D antiferromagnet. In the 3D antiferromagnet, with $K(0)$ set equal to $0.233J(0)$, there is a 1.54% deviation from full saturation of the expectation value $\langle S_z \rangle = \frac{5}{2}$. However in the quasi-1D antiferromagnet, with $K(0) = 0.002J(0)$, there is a massive 32% reduction. This huge zero-point motion at $T = 0$ K is very dependent on the magnetic anisotropic exchange parameter $K(0)$. This point is further illustrated in figure 2, which shows the zero-point motion of an $S = \frac{5}{2}$ ion, at $T = 0$ K, for various ratios of the exchange parameter η (J_b/J_a) and the magnetic anisotropy parameter $K(0)$. For example, if the 3D value of $K(0) = 0.233J(0)$ appropriate to $MnCl_2 \cdot 4H_2O$ is used, the zero-point motion drops to 5%. These results are compared in table 2 with results obtained using the spin-wave theory of Keffer (1966) and the results of Davis (1960) obtained using a cluster expansion model. In order to make direct comparison with Keffer (1966), the Green function calculations were obtained by (i) summing over a cubic Brillouin zone and (ii) using the full Brillouin zone boundary restrictions of equation (29).

From an examination of the results shown in table 2 it will be seen that the Green function calculations agree closely with the spin-wave theory of Keffer (1966) and qualitatively with the cluster expansion result of Davis (1960). With regard to the spin-wave result it can be shown that equation (28) for φ_2 at $T = 0$ K is exactly equal to the expression ΔM_{SO} for the magnetic deviation from saturation given by Keffer (1966). Thus in the low-temperature limit, the 3D Green function calculations must approach

Table 2. Predictions of the zero-point motion of an $S = \frac{5}{2}$ spin in 1D and 3D antiferromagnets[a].

	Spin wave	Green function theory		
	Keffer (1966, eqn (43.14))	Cubic BZ summation	Full BZ restrictions	Cluster theory Davis (1960)
Cubic $K(0) = 0$	3.12%	3.12%	3.36%	2.49%
Quasi-1D $K(0)/J(0) = 0.00215$ $J_b/J_a = 0.01$	22.0%	21.5%	32.4%	10.07% ↑ $K(0) = 0$ $J_b/J_a = 0$

[a] Note that the spin-wave calculation (using equation (43.14) of Keffer (1966)) and the cubic Green function summation, used a k-space summation over a cubic Brillouin zone. The full BZ boundary restriction calculation, however, used a k-space summation over a truncated octahedron for Brillouin zone.

the spin-wave results. In the case of the cluster expansion method however, Davis (1960) truncated the series expansion after the seventh order, but was unable to prove that this was sufficient. Indeed Keffer (1966) has noted that, for the linear chain, the seventh-order term is quite large. Thus the accuracy of the Davis estimates must be questioned. By way of contrast however, Green function theory includes all orders of interaction, at least within the RPA approximation. Thus the RPA model should provide the most accurate calculation, to date, of zero-point motion in a quasi-1D antiferromagnet. Finally, it should be noted that the spin-wave calculations of Keffer (1966) ignore the second boundary condition of equation (29). While this is probably a reasonable approximation for 3D antiferromagnets at very low temperatures, its validity for quasi-1D antiferromagnets is questionable.

In summary, therefore, we believe that quasi-1D antiferromagnets with low anisotropy will exhibit considerable zero-point motion. This phenomenon has immediate implications for the NO results in the quasi-1D antiferromagnet $CsMnCl_3 \cdot 2H_2O$, discussed in II. For example, the large transverse fluctuations in the electronic spins of the Mn^{2+} ions in $CsMnCl_3 \cdot 2H_2O$ associated with zero-point motion may be able to induce transitions in the nuclear levels, via the off-diagonal elements in the hyperfine interaction. This point will be raised again in II, in our discussion of the observed cooling rates in $CsMnCl_3 \cdot 2H_2O$.

The situation in external magnetic fields, directed along the easy magnetic axis, is summarised in figure 3. Note that the field-dependent AF-P phase transition is reached when one of the sublattice magnetisations $\langle S_z \rangle \rightarrow 0$. This information has been used to determine the phase diagrams shown in figure 4. It will be observed that the maximum in the AF-P transition occurs around $\tau = \tau_N/2$ where the largest changes in the specific heat induced by applied magnetic fields also occur. From the adiabatic magnetisation point of view therefore, maximum adiabatic cooling could be achieved in this region.

The calculated behaviour of the $\langle \hat{T}_0^1 \rangle_{1,2}$ shown in figure 3 also reveals that both sublattice magnetisations change significantly with applied field, particularly near the phase transition. In this region, therefore, the spin-wave approach of Gladkov (1986a, b) would be clearly inappropriate.

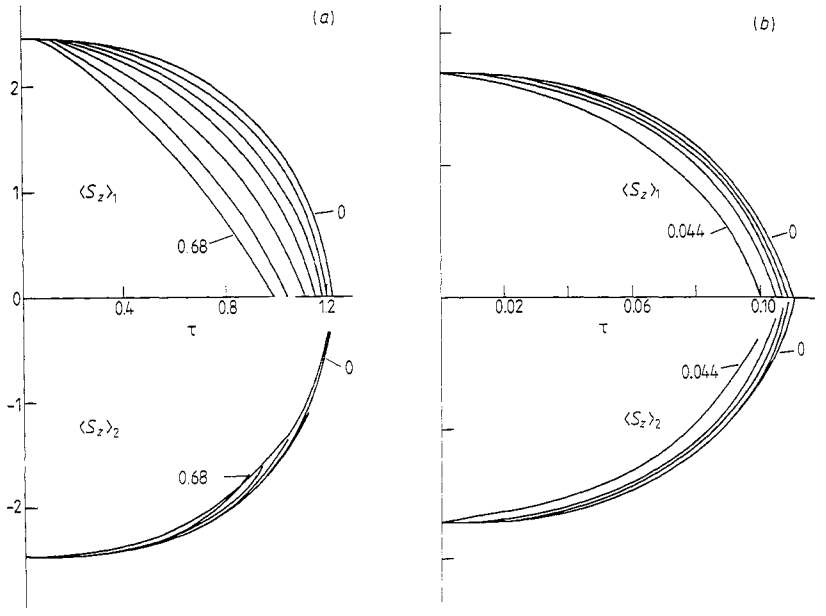

Figure 3. Calculated temperature dependence of the sublattice magnetisation in a 3D antiferromagnet (*a*), with $S = 5/2$ and $(J(0) + K(0))/J(0) = 1.233$, and a quasi-1D antiferromagnet (*b*), with $S = 5/2$ and $(J(0) + K(0))/J(0) = 1.00215$, in various applied fields, with $B_{app}/B_{eff} = 0, 0.12, 0.24, 0.36, 0.48, 0.60, 0.68$ for (*a*), and 0, 0.016, 0.024, 0.032, 0.044 for (*b*).

4.2. Entropy and specific heat

In the interpretation of NO experiments, the behaviour of the entropy and specific heat near field-induced phase transitions and their influence on the cooling rates of nuclear spins are of great importance. However, before we can use the RPA results presented earlier, there is a mathematical difficulty to be overcome.

The usual method of estimating the total energy of the magnons is based on the harmonic oscillator approximation. While this approximation is valid as $T \rightarrow 0$ K, it will overestimate thermodynamic quantities as the energy gap in the magnon excitations goes to zero. This of course is exactly what happens when $B_{app} \rightarrow B_{sf}$. One solution to this problem would be to use the harmonic oscillator description in low magnetic fields at low temperatures, while reverting to a simple renormalised effective-field model at higher temperatures. However, inevitably, there will be difficulties in interpolating between the two distinct models.

A simpler, more elegant, solution has been devised, which involves modifying the usual boson occupation number. Instead of writing

$$n_j(k) = [\exp(\beta E_{jk}) - 1]^{-1} \tag{31}$$

we define a quasi-boson occupation number

$$n_j(k) = \frac{1 - \exp[-(2S+1)\beta E_{jk}]}{\exp(\beta E_{jk}) - 1}. \tag{32}$$

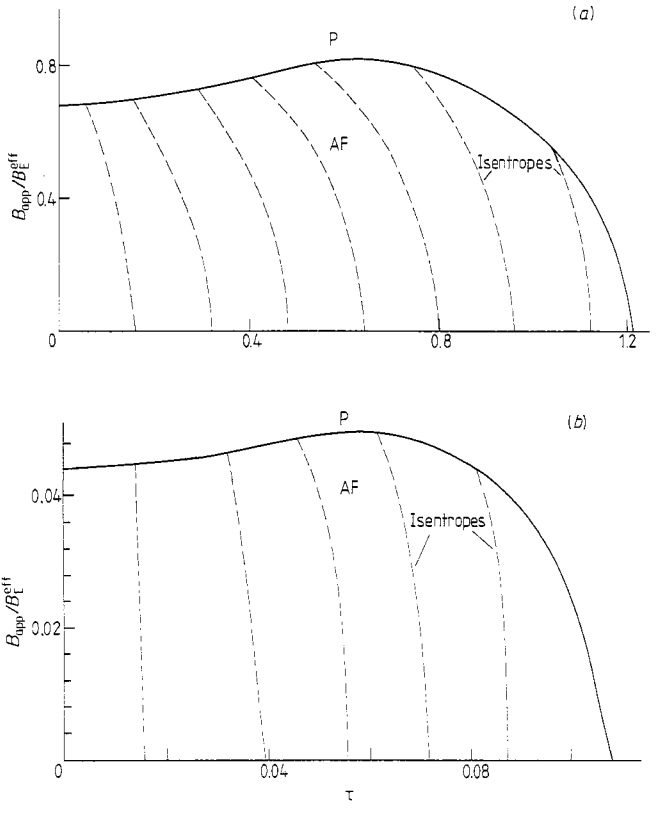

Figure 4. The magnetic phase diagram of a 3D antiferromagnet (*a*), with $S = 5/2$ and $(J(0) + K(0))/J(0) = 1.233$, and a quasi-1D antiferromagnet (*b*), with $S = 5/2$ and $(J(0) + K(0))/J(0) = 1.00215$, in the random-phase approximation.

With this simple change to the accepted harmonic oscillator description, it can be shown that the correct entropy and specific heat limits are obtained at both high and low temperatures (Martin 1987).

In this approximation, the entropy for the model antiferromagnet, for any B_{app} and T, is given by

$$S_{ent} = k_B \sum_k \sum_{j=1}^{2} \left[\ln\left(\frac{1 - \exp[-(2S+1)\beta E_{jk}]}{2\sinh(\beta E_{jk}/2)} \right) + \frac{\beta E_{jk}}{2} \coth\left(\frac{\beta E_{jk}}{2} \right) - \frac{\beta E_{jk}(2S+1)\exp[-(2S+1)\beta E_{jk}]}{1 - \exp[-(2S+1)\beta E_{jk}]} \right] \tag{33}$$

and the specific heat by

$$C_H = T\left(\frac{\partial S_{ent}}{\partial T} \right)_H . \tag{34}$$

Once again, for ease of computation, both the entropy and its temperature derivative were calculated using a coarse grid in the Brillouin zone. Consequently equation (33) was modified in similar fashion to equation (28), to preserve normalisation.

The calculated zero-applied entropy and specific heat behaviour are shown alongside the sublattice magnetisation curves in figure 1. Some calculations of possible temperature changes, following adiabatic magnetisation, are also shown in the phase diagrams of figure 4. As mentioned previously, this is the well known cooling effect predicted and observed experimentally by Joenk (1962).

In comparing the specific heat and entropy behaviour of a 3D antiferromagnet and quasi-1D antiferromagnet, in zero applied field (figure 1), it is apparent that the quasi-1D antiferromagnet has a lower magnon specific heat and entropy as $T \rightarrow 0$. This is in agreement with the experimental results for $CsMnCl_3 \cdot 2H_2O$ and $MnCl_2 \cdot 4H_2O$, determined by Kopinga *et al* (1975) and Miedema *et al* (1965), respectively. Further, the specific heat and entropy for the quasi-1D antiferromagnet in zero applied field are really only significant at τ_N. By way of contrast, the 3D antiferromagnet has a significant specific heat value down to $\tau_N/3$. Note that the maxima in the specific heat coincide with τ_N, as expected.

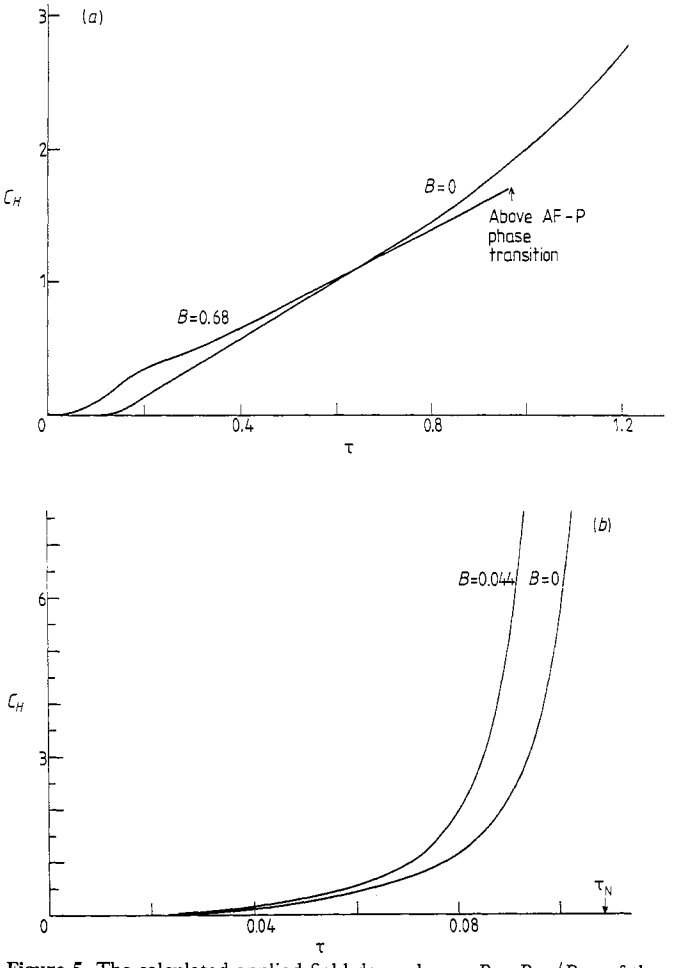

Figure 5. The calculated applied field dependence, $B = B_{app}/B_{eff}$, of the specific heat for a 3D antiferromagnet (*a*), with $S = 5/2$ and $(J(0) + K(0))/J(0) = 1.233$, and a quasi-1D antiferromagnet (*b*), with $S = 5/2$ and $(J(0) + K(0))/J(0) = 1.00215$.

The dependence of the specific heat on temperature for various applied fields is shown in figure 5. In both cases the specific heat near the field-induced phase transition is not orders of magnitude greater than that in zero applied field. Thus the specific-heat problem posed by Allsop *et al* (1984) remains. As a check on the reliability of these calculations, some experimental results on the specific heats of $MnCl_2 \cdot 4H_2O$ and $CsMnCl_3 \cdot 2H_2O$, in applied fields, have been compared with the Green function calculations. Giauque and Reichert (1969) and Giauque *et al* (1970) have provided some information for $MnCl_2 \cdot 4H_2O$ above 0.4 K, a region where the magnon–nuclear coupling can be expected to have negligible effect. These data, shown in figure 6, reveal only a 25% increase of the specific heat at B_{sf}, in reasonable agreement with the Green function calculation presented in figure 5(*a*). No experimental information is available for $CsMnCl_3 \cdot 2H_2O$, but data on other quasi-1D antiferromagnets, $(CH_3)_3NHMnX_3 \cdot 2H_2O$ where X = Cl, Br (Takeda *et al* 1982), reveal a considerable increase in the specific heat with increasing field just below T_N.

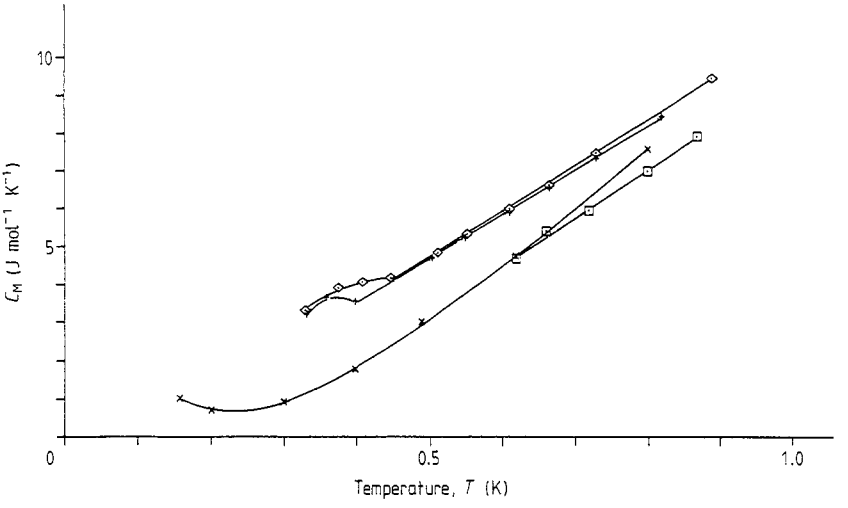

Figure 6. Experimental specific heat measurements for $MnCl_2 \cdot 4H_2O$, in various applied fields: Miedema *et al* (1965), $B_{app} = 0$ T (×); Giauque *et al* (1969), $B_{app} = 0$ T (□), 0.72 T (+) and 0.73 T (◇).

5. Two-sublattice antiferromagnet with hyperfine interactions

On including two nuclear sublattices four coupled Green function equations of motion are required, two electronic

$$E\langle\langle \hat{T}_1^1(l); \hat{T}_{q-1}^n(m)\rangle\rangle = c_1\langle \hat{T}_q^n(m)\rangle\delta_{l,m}/(2\pi) + g\mu_B B_{app}\langle\langle \hat{T}_1^1(l); \hat{T}_{q-1}^n(m)\rangle\rangle$$
$$+ \alpha(S)\sum_{j\neq l}\{(J_{lj} + K_{lj})\langle\langle \hat{T}_1^1(l)\hat{T}_0^1(j); \hat{T}_{q-1}^n(m)\rangle\rangle$$
$$- J_{lj}\langle\langle \hat{T}_0^1(l)\hat{T}_1^1(j); \hat{T}_{q-1}^n(m)\rangle\rangle\}$$
$$- \alpha(I)A[\langle\langle \hat{T}_1^1(l)\hat{L}_0^1(l); \hat{T}_{q-1}^n(m)\rangle\rangle - \langle\langle \hat{T}_0^1(l)\hat{L}_1^1(l); \hat{T}_{q-1}^n(m)\rangle\rangle] \qquad (35)$$

$$E\langle\langle \hat{T}_1^1(p); \hat{T}_{q-1}^n(m)\rangle\rangle = g\mu_B B_{app}\langle\langle \hat{T}_1^1(p); \hat{T}_{q-1}^n(m)\rangle\rangle + (S)\sum_{i\neq p}\{(J_{pi}+K_{pi})\langle\langle \hat{T}_1^1(p)\hat{T}_0^1(i); \hat{T}_{q-1}^n(m)\rangle\rangle - J_{pi}\langle\langle \hat{T}_0^1(p)\hat{T}_1^1(i); \hat{T}_{q-1}^n(m)\rangle\rangle\} - \alpha(I)A[\langle\langle \hat{T}_1^1(p)\hat{L}_0^1(p); \hat{T}_{q-1}^n(m)\rangle\rangle - \langle\langle \hat{T}_0^1(p)\hat{L}_1^1(p); \hat{T}_{q-1}^n(m)\rangle\rangle] \tag{36}$$

and two nuclear

$$E\langle\langle \hat{L}_1^1(l); \hat{T}_{q-1}^n(m)\rangle\rangle = g_N\mu_N B_{app}\langle\langle \hat{L}_1^1(l); \hat{T}_{q-1}^n(m)\rangle\rangle - \alpha(S)A[\langle\langle \hat{T}_0^1(l)\hat{L}_1^1(l); \hat{T}_{q-1}^n(m)\rangle\rangle - \langle\langle \hat{T}_1^1(l)\hat{L}_0^1(l); \hat{T}_{q-1}^n(m)\rangle\rangle] \tag{37}$$

$$E\langle\langle \hat{L}_1^1(p); \hat{T}_{q-1}^n(m)\rangle\rangle = g_N\mu_N B_{app}\langle\langle \hat{L}_1^1(p); \hat{T}_{q-1}^n(m)\rangle\rangle - \alpha(S)A[\langle\langle \hat{T}_0^1(p)\hat{L}_1^1(p); \hat{T}_{q-1}^n(m)\rangle\rangle - \langle\langle \hat{T}_1^1(p)\hat{L}_0^1(p); \hat{T}_{q-1}^n(m)\rangle\rangle] \tag{38}$$

where the $\hat{T}_q^n$ and $\hat{L}_q^n$ refer to the electronic and nuclear operators, respectively. Note that $\alpha(I)$ is given by equation (4) with S replaced by the nuclear spin I. As before l and p belong separately to sublattices (1) and (2), while $\alpha(S)$ and c_1 are given by equations (4) and (6) respectively. Note that it has been explicitly assumed that m and l lie on sublattice (1), and so the kernel term $c_1\langle\hat{T}_q^n(m)\rangle/(2\pi)$ appears only in equation (35).

To solve equations (35)–(38), it is necessary to find an expression for $\langle\langle \hat{T}_1^1(l); \hat{T}_{q-1}^n(m)\rangle\rangle$ and hence $\langle\hat{T}_q^n\rangle_1$. To obtain $\langle\hat{T}_q^n\rangle_2$ and $\langle\hat{L}_q^n\rangle_{1,2}$ three more sets of four coupled equations are required, where the $\hat{T}_{q-1}^n(m)$ operator has been replaced by $\hat{T}_{q-1}^n(n)$, $\hat{L}_{q-1}^n(m)$ and $\hat{L}_{q-1}^n(n)$ respectively, where n and p lie on sublattice (2). These equations are very similar to equations (35)–(38) except that the appropriate kernel term appears in the new parent equation of motion. For example, the equation of motion for $\langle\langle \hat{L}_1^1(p); \hat{L}_{q-1}^n(n)\rangle\rangle$ is the parent for $\langle\hat{L}_q^n\rangle_2$.

Once again the RPA is employed, and on taking the spatial Fourier transforms a 4×4 matrix equation is obtained

$$E\mathbf{G}^{ne} = \mathbf{N}\mathbf{G}^{ne} + \mathbf{V} \tag{39}$$

where (i) the 16 coupled, Fourier-transformed Green functions

$$\mathbf{G}^{ne} = \begin{bmatrix} G_{11}^{ee}(E,k) & G_{12}^{ee}(E,k) & G_{11}^{ne}(E,k) & G_{12}^{ne}(E,k) \\ G_{21}^{ee}(E,k) & G_{22}^{ee}(E,k) & G_{21}^{ne}(E,k) & G_{22}^{ne}(E,k) \\ G_{11}^{en}(E,k) & G_{12}^{en}(E,k) & G_{11}^{nn}(E,k) & G_{12}^{nn}(E,k) \\ G_{21}^{en}(E,k) & G_{22}^{en}(E,k) & G_{21}^{nn}(E,k) & G_{22}^{nn}(E,k) \end{bmatrix} \tag{40}$$

are defined in table 1, (ii) the matrix $\mathbf{N}$ is of the form

$$\mathbf{N} = \begin{bmatrix} M(1,1)+\alpha(I)A\rho_{0[1]}^1 & M(1,2) & \alpha(I)\langle\hat{T}_0^1\rangle_1 Q & 0 \\ M(2,1) & M(2,2)+\alpha(I)A\rho_{0[2]}^1 & 0 & \alpha(I)\langle\hat{T}_0^1\rangle_2 A \\ -\alpha(S)A\rho_{0[1]}^1 & 0 & g_N\mu_N B_{app}-\alpha(S)\langle\hat{T}_0^1\rangle_1 A & 0 \\ 0 & -\alpha(S)A\rho_{0[2]}^1 & 0 & g_N\mu_N B_{app}-\alpha(S)\langle\hat{T}_0^1\rangle_2 A \end{bmatrix} \tag{41}$$

(iii) the $M(i,j)$ terms appearing in equation (41) are purely electronic terms (see equation (11)) and (iv)

$$\mathbf{V} = \begin{bmatrix} c_1\langle \hat{T}_q^n \rangle_1/(2\pi) & 0 & 0 & 0 \\ 0 & c_1\langle \hat{T}_q^n \rangle_2/(2\pi) & 0 & 0 \\ 0 & 0 & c_2(-1)^{-n}\rho_{q[2]}^n/(2\pi) & 0 \\ 0 & 0 & 0 & c_2(-1)^{-n}\rho_{q[2]}^n/(2\pi) \end{bmatrix}. \quad (42)$$

Note that

$$\rho_{0[1]}^1 = (-1)^1\langle L_0^1 \rangle_1 \quad (43)$$

and

$$c_2 = -[(n+q)(n-q+1)/2]^{1/2}/\alpha(I) \quad (44)$$

in accordance with equation (6).

On solving equation (39) for $G_{11}^{ee}(E,k)$, $G_{22}^{ee}(E,k)$, $G_{11}^{nn}(E,k)$ and $G_{22}^{nn}(E,k)$ respectively, we find

$$G_{11}^{ee}(E,k) = \frac{c_1\langle \hat{T}_q^n \rangle_1}{2\pi\Delta}\left[E - \left(g\mu_B B_{app} + \alpha(S)\langle \hat{T}_0^1 \rangle_1[J(0)+K(0)] + \alpha(I)A\rho_{0[2]}^1 + \frac{\alpha(S)\alpha(I)A^2\langle \hat{T}_0^1 \rangle_2\rho_{0[2]}^1}{E - [g_N\mu_N B_{app} - \alpha(S)\langle \hat{T}_0^1 \rangle_2 A]}\right)\right] \quad (45)$$

$$G_{22}^{ee}(E,k) = \frac{c_1\langle \hat{T}_q^n \rangle_2}{2\pi\Delta}\left[E - \left(g\mu_B B_{app} + \alpha(S)\langle \hat{T}_0^1 \rangle_2[J(0)+K(0)] + \alpha(I)A\rho_{0[1]}^1 + \frac{\alpha(S)\alpha(I)A^2\langle \hat{T}_0^1 \rangle_1\rho_{0[1]}^1}{E - [g_N\mu_N B_{app} - \alpha(S)\langle \hat{T}_0^1 \rangle_1 A]}\right)\right] \quad (46)$$

$$G_{11}^{nn}(E,k) = \frac{c_2(-1)^{-n}\rho_{q[1]}^n}{2\pi\Delta\{E - [g_N\mu_N B_{app} - \alpha(S)\langle \hat{T}_0^1 \rangle_1 A]\}} \times \left(\Delta + \frac{\alpha(S)\alpha(I)A^2\langle \hat{T}_0^1 \rangle_1\rho_{0[1]}^1}{E - [g_N\mu_N B_{app} - \alpha(S)\langle \hat{T}_0^1 \rangle_1 A]}\right) \quad (47)$$

$$G_{22}^{nn}(E,k) = \frac{c_2(-1)^{-n}\rho_{q[2]}^n}{2\pi\Delta\{E - [g_N\mu_N B_{app} - \alpha(S)\langle \hat{T}_0^1 \rangle_2 A]\}} \times \left(\Delta + \frac{\alpha(S)\alpha(I)A^2\langle \hat{T}_0^1 \rangle_2\rho_{0[2]}^1}{E - [g_N\mu_N B_{app} - \alpha(S)\langle \hat{T}_0^1 \rangle_2 A]}\right) \quad (48)$$

where

$$\Delta = \left\{\left[E - \left(g\mu_B B_{app} + \alpha(S)\langle \hat{T}_0^1 \rangle_1[J(0)+K(0)] + \alpha(I)A\rho_{0[2]}^1 + \frac{\alpha(S)\alpha(I)A^2\langle \hat{T}_0^1 \rangle_2\rho_{0[2]}^1}{E - [g_N\mu_N B_{app} - \alpha(S)\langle \hat{T}_0^1 \rangle_2 A]}\right)\right] \times \left[E - \left(g\mu_B B_{app} + \alpha(S)\langle \hat{T}_0^1 \rangle_2[J(0)+K(0)] + \alpha(I)A\rho_{0[1]}^1 + \frac{\alpha(S)\alpha(I)A^2\langle \hat{T}_0^1 \rangle_1\rho_{0[1]}^1}{E - [g_N\mu_N B_{app} - \alpha(S)\langle \hat{T}_0^1 \rangle_1 A]}\right)\right] - \alpha^2(S)\langle \hat{T}_q^n \rangle_1\langle \hat{T}_q^n \rangle_2 J(k)J(-k)\right\}. \quad (49)$$

As before, the energies of the four coupled modes are given by the roots of the matrix **N**.

Given equations (45)–(49) the self-consistent calculation of the $\langle \hat{T}_q^n \rangle_{1,2}$ and $\rho^n_{q[1,2]}$ may be obtained in a similar manner to those of equations (17)–(22), using the inverse Fourier transform equations (17) and (18), together with their nuclear equivalents

$$\langle\langle \hat{L}_1^1(l); \hat{L}_{q-1}^n(m) \rangle\rangle = 2N^{-1} \sum_k G_{11}^{nn}(E, k) \exp[+i\boldsymbol{k} \cdot (\boldsymbol{R}_l - \boldsymbol{R}_m)] \tag{50}$$

$$\langle\langle \hat{L}_1^1(p); \hat{L}_{q-1}^n(n) \rangle\rangle = 2N^{-1} \sum_k G_{22}^{nn}(E, k) \exp[+i\boldsymbol{k} \cdot (\boldsymbol{R}_p - \boldsymbol{R}_n)]. \tag{51}$$

Once again use is made of the spectral theorem of Zubarev (1960), and the equilibrium correlation functions

$$\langle \hat{T}_{q-1}^n \hat{T}_1^1 \rangle_1 = c_1 \langle \hat{T}_q^n \rangle_1 \varphi_3 \tag{52}$$

$$\langle \hat{T}_{q-1}^n \hat{T}_1^1 \rangle_2 = c_1 \langle \hat{T}_q^n \rangle_2 \varphi_4 \tag{53}$$

$$\langle \hat{L}_{q-1}^n \hat{L}_1^1 \rangle_1 = c_1 (-1)^{-n} \rho^n_{q[1]} \varphi_5 \tag{54}$$

$$\langle \hat{L}_{q-1}^n \hat{L}_1^1 \rangle_2 = c_1 (-1)^{-n} \rho^n_{q[2]} \varphi_6 \tag{55}$$

where (i)

$$\varphi_i = \frac{2}{N} \sum_k \left(\frac{d_{1i}(k)}{\exp(\beta E_{1k}) - 1} + \frac{d_{2i}(k)}{\exp(\beta E_{2k}) - 1} + \frac{d_{3i}(k)}{\exp(\beta E_{3k}) - 1} + \frac{d_{4i}(k)}{\exp(\beta E_{4k}) - 1} \right) \tag{56}$$

and (ii) the $d_{ji}(k)$ are found by converting the energy-dependent terms in the RHS of equation (45) into partial fractions. Explicity

$$\begin{aligned} \frac{1}{\Delta} \Bigg[E - \alpha(S) \Bigg(& g\mu_B B_{app} + \langle \hat{T}_0^1 \rangle_1 [J(0) + K(0)] + A\rho^1_{0[2]} \\ & + \frac{\alpha(I) A^2 \langle \hat{T}_0^1 \rangle_2 \rho^1_{0[2]}}{E - \alpha(I)[g_N \mu_N B_{app} - \langle T_0^1 \rangle_2 A]} \Bigg) \Bigg] \\ \equiv & \frac{d_{11}(k)}{E - E_{1k}} + \frac{d_{21}(k)}{E - E_{2k}} + \frac{d_{31}(k)}{E - E_{3k}} + \frac{d_{41}(k)}{E - E_{4k}} \end{aligned} \tag{57}$$

where the E_{jk} are the coupled excitation energies of the Hamiltonian. The other constants $d_{j2}(k)$, $d_{j3}(k)$ and $d_{j4}(k)$ are obtained in a similar fashion, using the RHS of equations (46), (47) and (48), respectively.

As noted earlier the functional forms of equations (52)–(55) are equivalent to the solution for the ferromagnet discussed by Bowden *et al* (1986). Only the weighting factors φ_i have changed to reflect the presence of four coupled modes. However, although general analytic expressions for the eigenvalues and the $d_{ji}(k)$ can be obtained, their complexity precludes any useful discussion. Instead, the required quantities have been obtained numerically, using self-consistent calculations of the $\langle \hat{T}_0^1 \rangle_{1,2}$ and $\rho^1_{0[1,2]}$.

5.1. Electronic and nuclear sublattice magnetisations in the coupled regime

In a similar fashion to equation (23), the electronic sublattice magnetisation for $S = \frac{5}{2}$ is

given by

$$\langle \hat{T}^1_{0} \rangle_{1,2} = \frac{5 + 28\varphi_{3,4} + 63\varphi^2_{3,4} + 70\varphi^3_{3,4} + 35\varphi^4_{3,4}}{\sqrt{70}[(1 + \varphi_{3,4})^6 - \varphi^6_{3,4}]} \tag{58}$$

for the two sublattices, where φ_3 and φ_4 are defined in equation (56). The ^{55}Mn nuclei also have $I = \frac{5}{2}$ and so possess analogous expressions to those of equation (59). However the radioactive ^{54}Mn nuclei, with spin $I = 3$, have the axial component of their rank-one statistical tensor ($\alpha \langle I_z \rangle_{1,2}$) in the form

$$\rho^1_{0[1,2]} = \frac{-(3 + 20\varphi_{5,6} + 56\varphi^2_{5,6} + 84\varphi^3_{5,6} + 70\varphi^4_{5,6} + 28\varphi^5_{5,6})}{2\sqrt{7}[(1 + \varphi_{5,6})^7 - \varphi^7_{5,6}]} \tag{59}$$

where φ_5 and φ_6 are also defined in equation (56). In our calculations, we have assumed that the ^{54}Mn is 100% abundant. In practice, of course, the radioactive nuclei are quite dilute. However, the general properties of the nuclear–magnon coupling will still be exhibited.

The sublattice parameters used to compute the results shown in figure 7 are the same for the model 3D and quasi-1D antiferromagnets discussed earlier. Using the $MnCl_2.4H_2O$ data given by Allsop *et al* (1984), the relative hyperfine interaction strength for the model 3D antiferromagnet was set at $A/g\mu_B B^{\text{eff}}_E = -0.00662$. For the quasi-1D antiferromagnet however, $A/g\mu_B B^{\text{eff}}_E$ was set equal to -0.000284, since the absolute strength of the hyperfine interaction for Mn ions changes little with chemical environment.

Both the electronic and nuclear sublattice magnetisations in zero applied field can be seen in figure 7. Also included in these diagrams are estimates of the total entropy and specific heat, based on a model where the nuclei and magnon excitations are assumed to be decoupled. It will be observed that the sublattice magnetisations for both the 3D and quasi-1D antiferromagnets are generally unaffected. The only noticeable feature is the amplitude of the zero-point motion, which is slightly reduced by the presence of the nuclei. The nuclear magnetisations closely approximate those of a paramagnetic ion in a fixed magnetic field. This of course supports our previous comments on the localised nature of the nuclear energy excitations, particularly in low applied fields and at low temperatures. However, this is not the case near the AF–P phase transition.

5.2. *Frequency pulling*

As stated earlier, the RPA was chosen because it can be used to calculate coupled mode energies, in a consistent fashion. The $k = 0$ eigenvalues of the modes can be seen in figure 8, which shows the temperature dependence of the nuclear–magnon coupling, in zero applied field. From an examination of this diagram it is evident that the coupling increases, with the nuclear magnetisation, for both 3D and quasi-1D antiferromagnets. In essence, the off-diagonal terms in the hyperfine interaction $\boldsymbol{AI} \cdot \boldsymbol{S}$ push apart the nuclear and magnon excitation branches, leading to reduction in the Mn hyperfine field. However, in the case of the quasi-1D antiferromagnet, the reduction is much more pronounced, with changes as large as 15%. In practice, this implies that nuclear cooling in a quasi-1D antiferromagnet will become progressively more difficult in the mulli-kelvin regime, because the magnitude of the hyperfine field is decreasing with decreasing temperature. Using the results presented in figure 9(*b*) we estimate that the ^{54}Mn hyperfine field will decrease by about 6% in going from 70 mK to 30 mK in $CsMnCl_3 \cdot 2H_2O$.

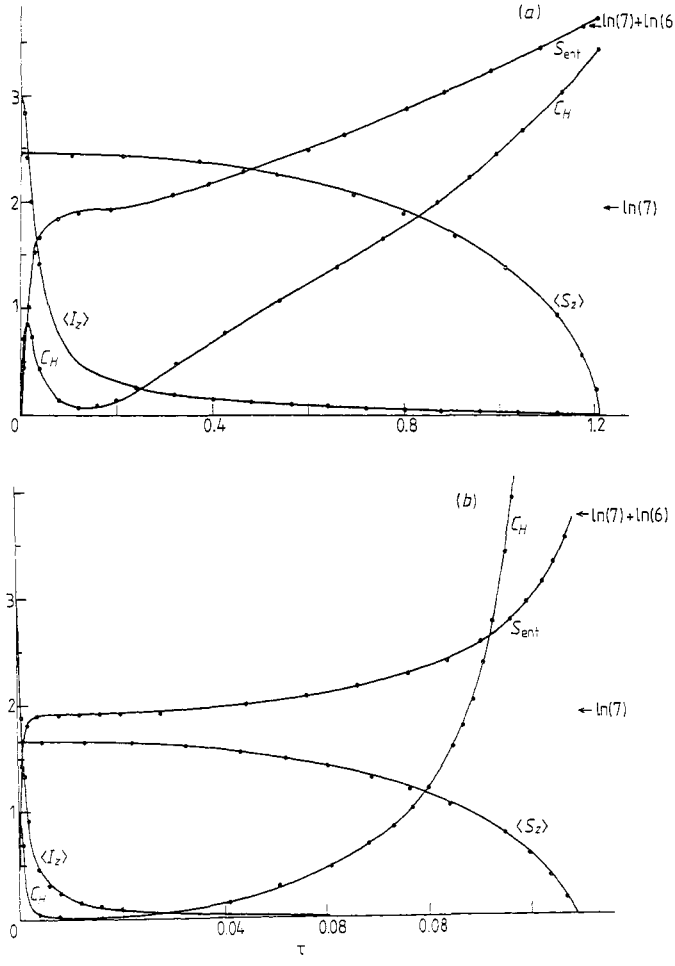

Figure 7. The calculated RPA results for a 3D antiferromagnet containing nuclei (*a*), with $S = 5/2$ and $(J(0) + K(0))/J(0) = 1.233$, and a quasi-1D antiferromagnet containing nuclei (*b*), with $S = 5/2$ and $(J(0) + K(0))/J(0) = 1.00215$, with $I = 3$ in both instances and the values of $A/g\mu_B B_E^{eff} - 0.00662$ and -0.000284 respectively.

The effect of nuclear–magnon repulsion becomes much more pronounced near the AF–P phase transition, as a result of the reduced energy gap in the magnon dispersion curve. The calculations shown in figure 9 reveal that the nuclear hyperfine splitting, at both sublattices, drops dramatically near the phase transition. This phenomenon, usually referred to as 'frequency pulling', has been witnessed experimentally for ^{51}V in V_3O_7 (Fujii *et al* 1983). Note, from a comparison of figures 9(*a*) and (*b*), that the reduction in the sublattice magnetisation, as a function of applied field, is much more pronounced in the quasi-1D antiferromagnet.

In general, the curvature of the magnetic hyperfine field, as a function of applied field, is similar to that found experimentally in $MnCl_2 \cdot 4H_2O$ (see Allsop *et al* 1984). However, while the change in the hyperfine splitting, predicted by the RPA model, is qualitatively similar to that observed in $MnCl_2 \cdot 4H_2O$, the Green function calculations do not fit the observed behaviour as well as the simple effective-field model used by

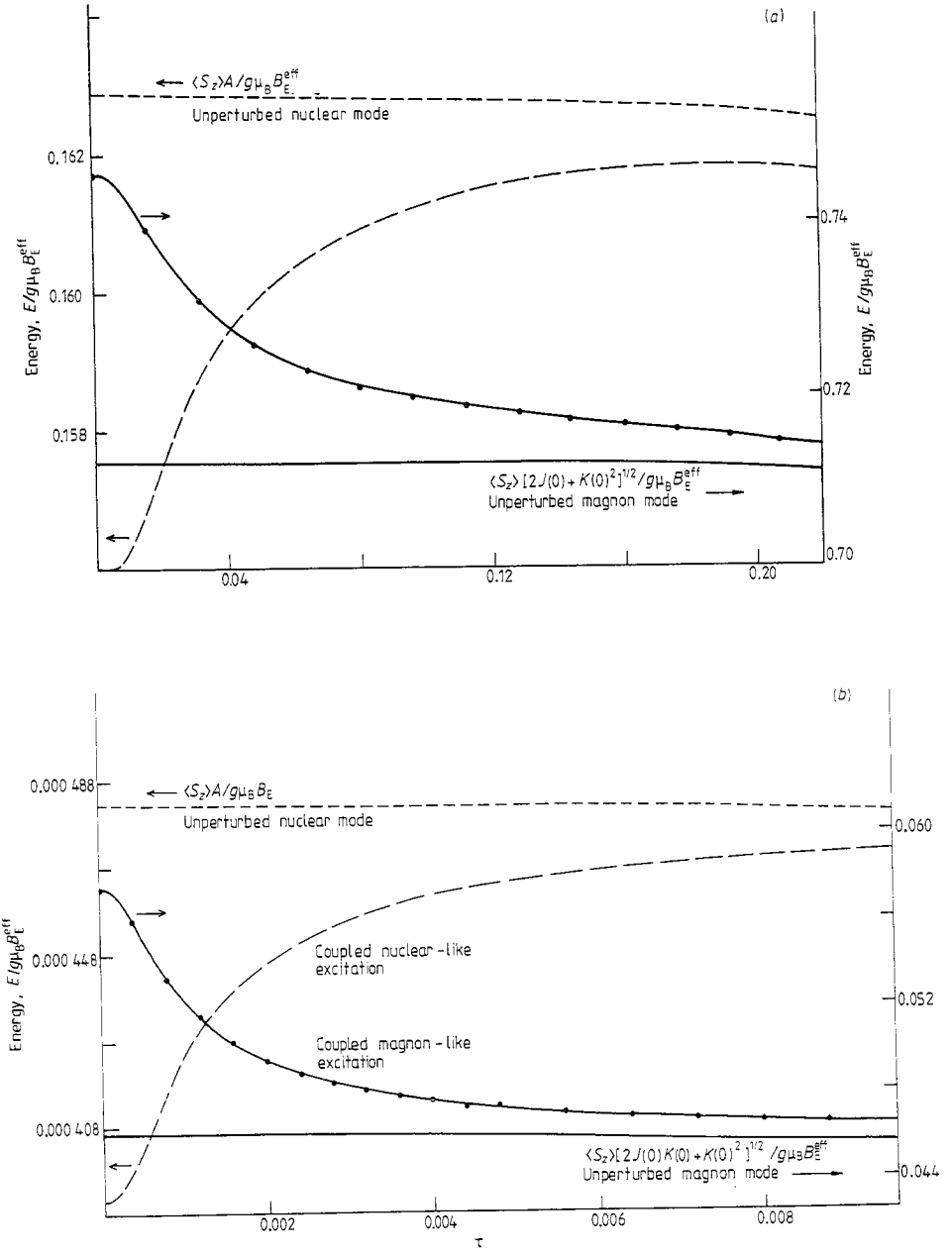

Figure 8. The calculated $k = 0$ energies of the coupled excitations, in zero applied field, for a 3D antiferromagnet (*a*) and a quasi-1D antiferromagnet (*b*), conditions for (*a*) and (*b*) as for figure 7.

Allsop *et al* (1984) and Martin (1987). In the RPA model the magnetic hyperfine field drops more quickly with increasing magnetic field than that found experimentally in $MnCl_2 \cdot 4H_2O$. This may be due to our choice of the $K(0)$ and $J(0)$ parameters. For example, a larger value of $K(0)$ would lead to a slower decrease in the hyperfine splitting,

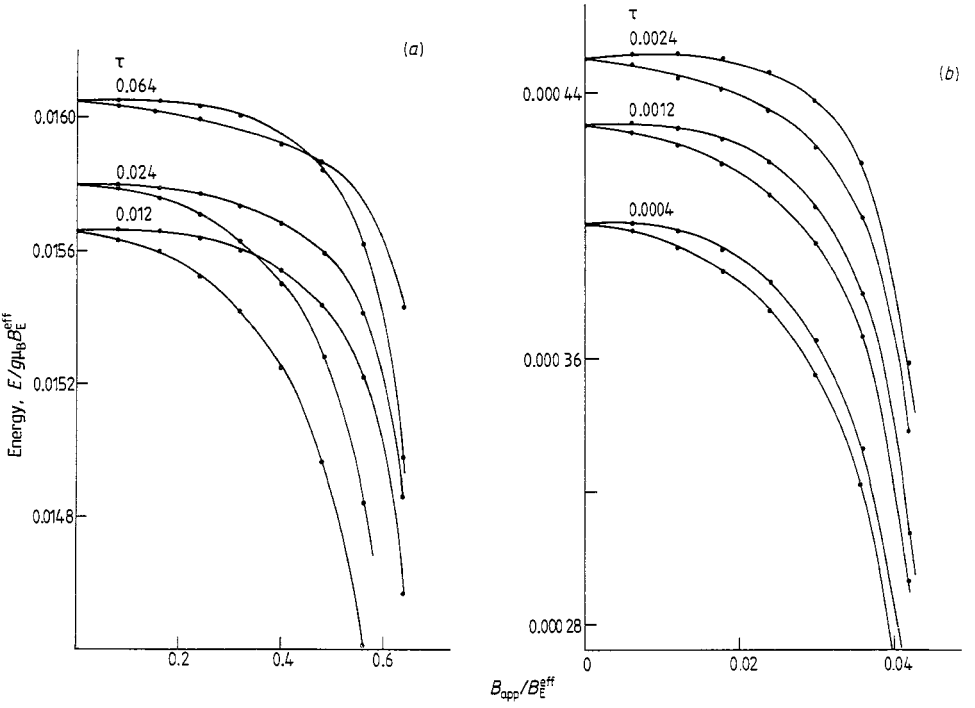

Figure 9. The calculated applied field dependence of the $k = 0$ nuclear excitations for a 3D antiferromagnet (*a*) and a quasi-1D antiferromagnet (*b*), conditions as for figure 7.

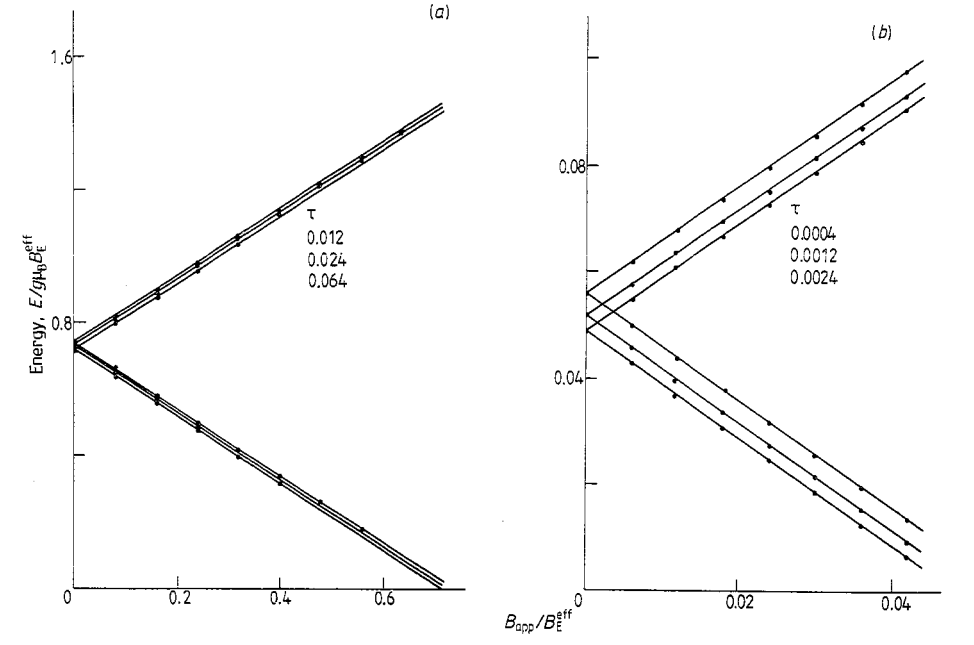

Figure 10. The calculated applied field dependence of the $k = 0$ magnon excitations for a 3D antiferromagnet (*a*) and a quasi-1D antiferromagnet (*b*), conditions as for figure 7.

with increasing applied field. The other main omission of the Green function calculations, of course, is the absence of a quadrupole interaction. Unfortunately, the RPA model cannot be modified to include quadrupole interactions, for the reasons given by Bowden *et al* (1986).

For completeness, we have also calculated the changes in the magnon mode energies of the two model antiferromagnets, shown in figure 10. While the zero-field frequency pulling causes a systematic shift in the magnon frequencies the general linear applied field dependence is still present, until close to the phase transition. The lifting of the magnon frequencies, above their unperturbed values, is, of course, due to the anti-crossing behaviour exhibited by coupled modes.

Finally, it should be admitted that we have been unable to compute the entropy of the coupled magnon–nuclei system near the AF-P transition. In zero applied field, the nuclei and the magnons are essentially decoupled, so it is permissible to write

$$S_{\text{tot}} = S_{\text{nuclei}} + S_{\text{magnons}}. \tag{60}$$

However, equation (60) must fail in the strong-coupling limit. Unfortunately, it is difficult to devise a suitable model, perhaps based on the assumption discussed in § 4.2, to compute the entropy of nuclear–magnon mixing.

6. Conclusions

Through the use of Green function theory it has proved possible to investigate the effect of magnon–nuclei coupling, right up to the AF-P transition. The results have shown that significant differences between 3D and quasi-1D antiferromagnets can be anticipated. In particular, it would appear that quasi-1D antiferromagnets with low anisotropy will be characterised by a larger zero-point motion, resulting in Mn moments some 30% below their saturation value at $T = 0$ K. This observation has immediate implications for NO and NMRON experiments on quasi-1D antiferromagnets. In the first place it is likely that the measured γ-ray anisotropies from quasi-1D antiferromagnets are likely to be considerably less than their 3D counterparts, because of their reduced hyperfine fields. Secondly, it is possible that the large transverse motion, associated with the large zero-point motion, will induce nuclear spin transitions and so give rise to a finite cooling rate, even in zero applied field. Both these possibilities, and others, are raised again in the following paper which gives details of a ^{54}Mn NO study of the quasi-1D antiferromagnet $CsMnCl_3 \cdot 2H_2O$.

Acknowledgments

GJB would like to thank both the Australian Research Grants Scheme and the University of New South Wales for financial assistance during the course of this work. JPDM would like to thank the Commonwealth Department of Education for a Post-Graduate Research Award.

References

Allsop A L, de Araujo M, Bowden G J, Clark R G and Stone N J 1984 *J. Phys. C: Solid State Phys.* **17** 915–37
Bowden G J, Martin J P D, Andrikidis C and Tainsh R J 1989 *J. Phys.: Condens. Matter* at press

Bowden G J, Martin J P D and Oitmaa J 1986 *J. Phys. C: Solid State Phys.* **19** 551–61
Bowden G J, Martin J P D, Stone N J, Andrikidis C and Tainsh R J 1987 *J. Phys. C: Solid State Phys.* **20** 4657–67
Butterworth G J, Woollam J A and Aron P 1973 *Physica* **70** 547–62
Davis H L 1960 *Phys. Rev.* **120**(3) 789–801
de Groot H J M and de Jongh L J 1986 *Physica* **141B** 1–36
Egami T and Brooks M S S 1975 *Phys. Rev.* B **12** 1021–8, 1029–37
Fujii M, Nishihara H and Hirai A 1983 *J. Phys. Soc. Japan* **52**(1) 272–8
Giaugue W F, Fisher A, Brodale G E and Hornung E W 1970 *J. Chem. Phys.* **52**(6) 2901–18
Giauque W F and Reichert T A 1969 *J. Chem. Phys.* **50**(10) 4205–22
Gladkov S O 1986a *Phys. Rep.* **132**(6) 277–365
—— 1986b *Phys. Rep.* **139**(3) 159–200
Haley S B 1978 *Phys. Rev.* B **17** 337–46
Joenk R J 1962 *Phys. Rev.* **128**(4) 1634–45
Keffer F 1966 *Handbuch der Physik* vol 18, pt 2 (Berlin: Springer) pp 1–273
Kopinga K, de Neef T and de Jonge W J M 1975 *Phys. Rev.* B **11**(6) 2364–9
Kubo R 1952 *Phys. Rev.* **87**(1) 568–80
Martin J P D 1987 *PhD Thesis* University of New South Wales
Miedema A R, Wielinga R F and Huiskamp W J 1965 *Physica* **31** 835–44
Rives J E and Benedict V 1975 *Phys. Rev.* B **12**(5) 1908–19
Skalyo J Jr, Shirane G, Friedberg S A and Kobayashi H 1970a *Phys. Rev.* B **2**(5) 1310–17
—— 1970b *Phys. Rev.* B **2**(11) 4632–35
Steffen R M and Alder K 1975 *The Electromagnetic Interaction in Nuclear Spectroscopy* (Amsterdam: North-Holland) ch 12
Takeda K, Koike T, Harada I and Tonegawa T 1982 *J. Phys. Soc. Japan* **51**(1) 85–93
Turrell B G 1985 *Hyp. Int.* **22** 187–92
Turrell B G, Kotlicki A and Le Gros M 1987 *Hyp. Int.* **36** 161–70
Zubarev D N 1960 *Sov. Phys.–Usp.* **3** 320–45